Biophysical Journal
Article

Biophysical Society

Efficient Multiscale Models of Polymer Assembly

Alvaro Ruiz-Martinez,[1] Thomas M. Bartol,[2] Terrence J. Sejnowski,[2,3,4,*] and Daniel M. Tartakovsky[1,*]
[1]Department of Mechanical and Aerospace Engineering, University of California-San Diego, La Jolla, California; [2]Computational Neurobiology Laboratory and [3]Howard Hughes Medical Institute, Salk Institute for Biological Studies, La Jolla, California; and [4]The Division of Biological Studies Sciences, University of California-San Diego, La Jolla, California

ABSTRACT Protein polymerization and bundling play a central role in cell physiology. Predictive modeling of these processes remains an open challenge, especially when the proteins involved become large and their concentrations high. We present an effective kinetics model of filament formation, bundling, and depolymerization after GTP hydrolysis, which involves a relatively small number of species and reactions, and remains robust over a wide range of concentrations and timescales. We apply this general model to study assembly of FtsZ protein, a basic element in the division process of prokaryotic cells such as *Escherichia coli*, *Bacillus subtilis*, or *Caulobacter crescentus*. This analysis demonstrates that our model outperforms its counterparts in terms of both accuracy and computational efficiency. Because our model comprises only 17 ordinary differential equations, its computational cost is orders-of-magnitude smaller than the current alternatives consisting of up to 1000 ordinary differential equations. It also provides, to our knowledge, a new insight into the characteristics and functioning of FtsZ proteins at high concentrations. The simplicity and versatility of our model render it a powerful computational tool, which can be used either as a standalone descriptor of other biopolymers' assembly or as a component in more complete kinetic models.

INTRODUCTION

Shape and internal organization of cells is regulated by the cytoskeleton, a three-dimensional meshwork of filamentous proteins that also provides mechanical support for essential processes such as cell division, motility, and intracellular transport (1–5). In a cell's cytoplasm, interacting monomers form long polymers called "filaments", which assemble and disassemble dynamically by elongation and annealing mechanisms. These filaments attach to the cell's membrane and constitute fundamental building elements of the cytoskeleton. Their arrangement into bundles contributes to the stability and strength of the network (6,7). In eukaryotic cells, both actin-based microfilaments and tubulin-based microtubules form bundles of different characteristics (8–11). For example, cell migration due to filopodia formation is regulated by the polymerization of long and tight filaments and by their subsequent bundling (8,12). Another example is F-actin polymerization and bundling, both of which are critical processes in birth, growth, and final form of mushroom-shaped dendritic spines as well as in the guidance and migration of neuronal growth cones (12–15). In prokaryotic cells such as *Escherichia coli* or *Bacillus subtilis*, FtsZ and MreB proteins (homologs of eukaryotic tubulins and actins) are the most dominant components of their cytoskeletons. Whereas FtsZ is responsible for division process, MreB controls the cell width. Different types of filaments and bundles of these proteins have been studied in vitro (16–18) and in vivo (19–21). In both eukaryotic and prokaryotic cells, continuous turnover of monomers between the cytosol and the network of polymers regulates the shape and size of filaments and bundles (13,14,22–24). Assembly and disassembly of polymers are, therefore, permanent activities even in the steady state.

Cytoskeletal ring formation, of which FtsZ protein is the main agent, is a key part of prokaryotic cell division. In the cytosol of, e.g., *E. coli*, FtsZ monomers diffuse freely and form no structures as long as they remain bound to guanosine diphosphate (GDP). Interactions with guanosine triphosphate (GTP) initiate polymerization of FtsZ monomers. The resulting protofilaments then attach themselves to the cell membrane, a process facilitated by FtsA and ZipA proteins (25–28). In both the cytosol and membrane, these protofilaments elongate, anneal, bundle, and form complex structures, such as entanglements and cross links. The in vitro experiments (29–31) suggest that proteins, such as ZapA or ZapB, reinforce the lateral bonds between filaments and bundles. Several positive and negative regulators of ring formation ensure that all of these processes take place in the center of the cell. A chain of several proteins (MatP, ZapA, and ZapB) in the replication terminus region (Ter macrodomain) promotes Z-ring formation at the midcell (32–34). Both Min

Submitted December 3, 2015, and accepted for publication May 9, 2016.
*Correspondence: terry@salk.edu or dmt@ucsd.edu
Editor: Dennis Bray.
http://dx.doi.org/10.1016/j.bpj.2016.05.022

proteins, which oscillate between the two poles of a cell (35–37), and SlmA proteins, involved in nucleoid occlusion (38,39), inhibit polymerization everywhere except at the midcell (40–43). Once the Z-ring structure forms in that location, it remains stable for several minutes (44), during which time there is still a continuous exchange of monomers between the cytoplasm and the FtsZ structure (22,23). This exchange increases the scaffold's robustness by modifying and repositioning the filaments. After that time, once the two new nucleoids are separated, contraction of the Z-ring is triggered, leading to the cell's division (45–48).

The in vitro experiments (22,23,28,41,49,50) provide further insight into the properties of FtsZ filaments. They established the existence of a critical concentration at which FtsZ monomers begin to polymerize; this critical concentration coincides with the concentration of FtsZ monomers observed in steady state. They showed that hydrolysis-induced turnover between FtsZ monomers in the pool and in the polymers/bundles network occurs at a constant rate in steady state; this phenomenon was also observed in vivo (51). When the total concentration of FtsZ monomers in all forms (C_{tot}) is high enough to observe bundle formation, this turnover remains practically the same for higher C_{tot} (22,52). Finally, they showed that while filaments have different lengths at different concentrations (23,50), the formation of bundles occurs only at high concentrations (22,23,53–55).

The importance and ubiquity of polymer assembly provided an impetus for development of kinetics models of these processes. A number of these models (22,45,50,56,57) aim to describe the in vivo and in vitro observations of FtsZ assembly. Initial stages of FtsZ polymerization have been adequately captured with the eight-equation model (22,50). The latter describes only the first seconds of polymerization for different FtsZ strains and buffer conditions, rather than the whole process of FtsZ assembly. The model's failure to handle later times and in vivo FtsZ concentrations stems from its inability to account for hydrolysis effects and transformations of filaments and bundles. Current models of full FtsZ assembly, e.g., those of Dow et al. (45), Lan et al. (56), and Surovtsev et al. (57), employ hundreds or even thousands of rate equations. Despite their complexity, most of them find it necessary to oversimplify the kinetics of hydrolysis and formation and dissociation of bundles, the processes that are known to be important at high concentrations of FtsZ protein found in living cells. Table 1 provides a comparison of these models in terms of their complexity, applicability range, and ability to predict the salient features of FtsZ assembly observed by Chen and Erickson (22) and Chen et al. (50).

We present a model of FtsZ assembly that ameliorates many of the shortcomings of its existing counterparts. It consists of only 17 equations, yet is capable of capturing the main characteristics of the in vitro experiment conducted by Chen and Erickson (22) over a wide range of FtsZ concentrations. The predictive accuracy of our model exceeds that of the more complex models (see Table 1). The significantly reduced complexity of our model stems from its reliance on an average length of filaments and bundles, rather than on a length distribution of different polymers. The initial stages of FtsZ assembly are described in our model with the eight rate equations introduced in Chen et al. (50).

This article is organized as follows. In Materials and Methods, we formulate a model of FtsZ assembly in terms of relevant unimolecular and bimolecular reactions and provide details on model parameterization, i.e., on selection of values of the reaction rates. In Results and Discussion, we discuss the predictions and insights provided by our model, as well as its advantages over several other models. Major conclusions from our study are summarized in the final section.

MATERIALS AND METHODS

Model of FtsZ assembly

We use coarse-graining to reduce all different sizes of polymers to a species called a filament, whose average length is tracked in time during the entire process. The resulting coarse-grained model comprises 17 ordinary differential equations (ODEs).

TABLE 1 Comparison of the Kinetic In Vitro Models in Terms of Their Complexity, Applicability Range, and Ability to Predict the Observed Features of FtsZ Assembly

	Refs. (22,50)	M1, Ref. (56)	M2, Ref. (56)	M3, Ref. (56)	Ref. (57)	Our Model
Number of ODEs	8	500	500	1254	300	17
Short time	yes	yes	yes	yes	yes	yes
Long time	no	yes	yes	yes	yes	yes
Low C_{tot}	yes	yes	yes	yes	yes	yes
High C_{tot}	no	no	no	no	yes	yes
Filament length	no	yes	yes	average^{+}	yes	average
Bundle width	no	no	two filaments	distribution^{+}	no	distribution
C_{cr}^{1}	yes^{-}	yes	yes	yes	yes^{-}	yes
C_{cr}^{2}	no	no	no	no	no	yes

M1, M2, and M3 designate the single-filament, two-filament-bundling, and multifilament-bundling models introduced in Lan et al. (56), respectively; C_{tot} is the total concentration of FtsZ monomers in all forms; low and high C_{tot} refers to its values of 2 and 10 μM, respectively; $C_{cr}^{1} = [Z^{na}]_{ss} + [Z]_{ss} = 0.7$ μM is the critical concentration at which polymerization begins, which is computed as the sum of the steady-state concentrations of nonactivated (GDP-bound) and activated (GTP-bound) FtsZ monomers, respectively; and $C_{cr}^{2} \approx 3.0$ μM is the critical value of concentration C_{tot} at which bundling becomes pronounced. The superscripts ($^{+}$) and ($^{-}$) denote the overestimated and underestimated predictions, respectively.

FIGURE 1 Basic polymer structures and reactions and their graphical representation. To see this figure in color, go online.

Model formulation

The first critical concentration C_{cr}^1 is the minimum concentration of FtsZ proteins in the monomeric form at which polymerization begins, and it establishes two regimes of polymerization. The first regime, $C_{tot} \leq C_{cr}^1$, admits only monomers such that $[Z^{na}] + [Z] \approx C_{tot}$, where $[Z^{na}]$ and $[Z]$ denote concentrations of nonactivated (GDP-bound) and activated (GTP-bound) FtsZ monomers, respectively. The second regime, $C_{tot} > C_{cr}^1$, allows for FtsZ polymerization and bundling, with $C_{cr}^1 = 0.7$ μM, in accordance with the experimental evidence in Chen and Erickson (22). The analysis presented below is concerned with the second regime of polymerization.

Let Z^{na} and Z denote a nonactivated (GDP-bound) and activated (GTP-bound) monomer, respectively. The first five polymers obtained by combining the corresponding number of monomers are denoted by Z_i, where $i = 2,\ldots, 6$. Longer polymers (i.e., filaments) are denoted by F. Bundles of k filaments are denoted by B_k, where $k = 2,\ldots, N$ and N is the maximum number of filaments in a bundle; it is allowed to increase with the total concentration of FtsZ monomers in all forms, C_{tot}. We show in Section S1 of the Supporting Material that $N = 10$ even in the physiologically extreme case of $C_{tot} = 10.0$ μM, i.e., our model relies on 17 species and equations to capture the process of FtsZ assembly. The basic structures (monomers, short polymers, filaments, and bundles) and their graphical representations are summarized in Fig. 1.

To avoid unphysical oversimplifications, we express the kinetics of the processes involved in FtsZ assembly, from its nonactivated monomeric form to long bundles of filaments, in terms of fundamental unimolecular

and bimolecular reactions. The process of activation is described by a reaction

$$Z^{\mathrm{na}} \underset{k_{\mathrm{ac}}^{-}}{\overset{k_{\mathrm{ac}}^{+}}{\rightleftharpoons}} Z, \tag{1}$$

with forward and backward reaction rates k_{ac}^{+} and k_{ac}^{-}, respectively. Activation and deactivation of monomers occurs due to their interactions with GTP and GDP nucleotides, respectively, even though GTP and GDP are not represented explicitly in our model. The process of nucleation is represented by a reaction

$$Z + Z \underset{k_{\mathrm{nu}}^{-}}{\overset{k_{\mathrm{nu}}^{+}}{\rightleftharpoons}} Z_2, \tag{2}$$

where k_{nu}^{+} and k_{nu}^{-} are the forward and backward reaction rates, respectively. Formation of nucleus of two monomers (nucleation or dimerization) is a critical stage of initialization of the FtsZ assembly (50); it also determines the rate of assembly of the polymer network. The elongation process is modeled by a set of reactions

$$Z + Z_i \underset{k_{\mathrm{el}}^{-}}{\overset{k_{\mathrm{el}}^{+}}{\rightleftharpoons}} Z_{i+1}, \quad i = 2, \ldots, 5, \tag{3a}$$

$$Z + Z_6 \xrightarrow{k_{\mathrm{el}}^{+}} F, \tag{3b}$$

$$Z + F_{z^-} \underset{k_{\mathrm{el}}^{-}}{\overset{k_{\mathrm{el}}^{+}}{\rightleftharpoons}} F_{z^+}, \tag{3c}$$

with forward and backward reaction rates k_{el}^{+} and k_{el}^{-}, respectively.

The reactions defined above comprise the activation-nucleation-elongation model proposed by Chen and Erickson (22), and used in Frieden and Goddette (58), Sept et al. (59)), and Falzone et al. (60) to describe the kinetics of actin polymerization. (These and other models, e.g., those of Chen and Erickson (22) and Lan et al. (56), use the notation $Z + F \rightleftharpoons F$ in which a filament before and after elongation process is denoted by the same letter. To differentiate between reactant-filaments and product-filaments in a given reaction, we introduce subscripts that clarify the physical processes that these reactions represent. Thus, in Eq. 3c, F_{z^-} and F_{z^+} designate a filament F before and after the attachment of a monomer Z, respectively. The forward reaction implies a decrement of the concentration of activated monomers $[Z]$ with the rate $-k_{\mathrm{el}}^{+}[Z][F_{z^-}]$. Similarly, the backward reaction represents the increment of the concentration of activated monomers with the rate $k_{\mathrm{el}}^{-}[F_{z^+}]$. Like the aforementioned models, our model assumes that all filaments are present in the same concentration regardless of their length, such that $[F_{z-}] = [F_{z+}] = [F]$. Section S1 extends this assumption to other species and reactions to reduce the number of ODEs.) We posit that their model, including its values of the reaction rate constants, is sufficient to describe short-time kinetics and, hence, adopt it as a module in our model. This module is supplemented with models of filament annealing, bundling of both filaments and bundles, and hydrolysis/dissociation reactions to handle long-time kinetics, as described below. We assume that filaments and bundles have the same length when they connect laterally and that bundles grow laterally in structures of two dimensions. With these simplifications, the process of filament annealing is represented by a reaction

$$F_{f^-} + F_{f^-} \underset{k_{\mathrm{an}}^{-}}{\overset{k_{\mathrm{an}}^{+}}{\rightleftharpoons}} F_{f^+}, \tag{4}$$

where k_{an}^{+} and k_{an}^{-} are forward and backward reaction rates, respectively; and the subscripts f^- and f^+ designate a filament F before and after the attachment of another filament F. The process of filament bundling consists of reactions

$$F + F \underset{k_{\mathrm{bu}}^{-}}{\overset{k_{\mathrm{bu}}^{+}}{\rightleftharpoons}} B_2, \tag{5a}$$

$$F + B_i \underset{k_{\mathrm{bu}}^{-}}{\overset{k_{\mathrm{bu}}^{+}}{\rightleftharpoons}} B_{i+1}, \quad i = 2, \ldots, N-1, \tag{5b}$$

$$B_i + B_j \underset{k_{\mathrm{bu}}^{-}}{\overset{k_{\mathrm{bu}}^{+}}{\rightleftharpoons}} B_{i+j}, \quad i+j = 4, \ldots, N, \tag{5c}$$

where k_{bu}^{+} and k_{bu}^{-} are the forward and backward reaction rates. The latter rate varies with $\overline{L}_{\mathrm{fb}}^{m}$, an average length of filaments of m monomers (or bundles made of filaments of m monomers), i.e., $k_{\mathrm{bu}}^{-} = k_{\mathrm{bu}}^{-}(\overline{L}_{\mathrm{fb}}^{m})$.

Two mechanisms contribute to the turnover of monomers between the solution and the network of filaments and bundles: hydrolysis of filaments and hydrolysis of bundles. The GTP-bound FtsZ monomers, which constitute the polymer network, exchange their nucleotides to GDP by hydrolysis. Subsequently, those monomers can detach from a filament or a bundle, restarting the polymerization process. In our model, dissociation of monomers from filaments after GTP hydrolysis involves two reactions

$$F_{z^+} \xrightarrow{k_{\mathrm{hy/dis}}^{1}} F_{z^-} + Z^{\mathrm{na}}, \tag{6a}$$

$$F_{z^+ f^+} \xrightarrow{k_{\mathrm{hy/dis}}^{2}} F_{z^- f^-} + Z^{\mathrm{na}} + F_{z^- f^-}, \tag{6b}$$

with reaction rates $k_{\mathrm{hy/dis}}^{1}$ and $k_{\mathrm{hy/dis}}^{2}$, and dissociation of monomers from bundles after GTP hydrolysis also consists of two reactions,

$$B_{i;z^+,b^+} \xrightarrow{k_{\mathrm{hy/dis}}^{2}} B_{i;z^-,b^-} + Z^{\mathrm{na}} + B_{i;z^-,b^-}, \quad i = 2, 3, \tag{7a}$$

$$B_{i;z^+} \xrightarrow{k_{\mathrm{hy/dis}}^{3}} B_{i;z^-} + Z^{\mathrm{na}}, \quad i = 2, \ldots, N, \tag{7b}$$

where $k_{\mathrm{hy/dis}}^{3}$ is a reaction rate. It is worthwhile noting that the depolymerization process described by Eqs. 6a and 6b ignores depolymerization of the first oligomers Z_2,..., Z_6. GTP hydrolysis does not affect either nucleation or first elongation phases because it occurs slowly, after the entry of a FtsZ subunit into a filament (22,52). For longer filaments, GTP hydrolysis precedes the loss of a nonactivated monomer from one of their ends, Eq. 6a, or even their middle, Eq. 6b (28,61). Equation 7a represents the loss of a monomer that links both sides of a bundle; it implies a decrement of the bundle length (only applied to thin bundles of two or three filaments). Equation 7b represents bundles that lose nonactivated monomers from their middle or from their ends after GTP hydrolysis, without significantly changing their dimensions (41). The subscripts $z^{\pm}$, $f^{\pm}$, and $b^{\pm}$ indicate the loss or gain of monomers, filaments, and bundles, respectively, i.e., indicate variations in the concentrations of the corresponding species.

Our model does not provide explicit information about the binding sites where these species attach or detach. Fig. 2 illustrates the actual process of shortening of a thin bundle after GTP hydrolysis and its simplified version implemented in our model. First, a bundle loses a GDP-bound FtsZ monomer somewhere in its middle after GTP hydrolysis (a process represented by Eq. 7b). Then, the same reaction can involve a monomer of the adjacent filament next to the position of the departed monomer, yielding two

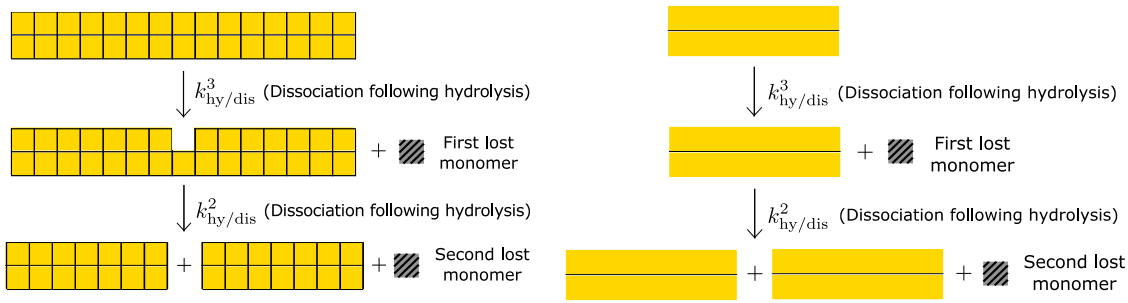

FIGURE 2 Shortening of a bundle of two filaments by hydrolysis (*left*) and its mathematical representation in our model (*right*). To see this figure in color, go online.

separated and shorter bundles (a process described by Eq. 7a). An explicit description of these two processes would give information about the location of the monomers before they leave the bundle and the length of the new bundles. Our model lacks these details, providing information only about concentrations of both monomers and bundles (hence, the subscripts $z^{\pm}$ and $b^{\pm}$ in Eqs. 7a and 7b).

Finally, attachment of monomers to bundles is represented by a reaction

$$Z + B_{i;z^-} \xrightarrow{k_{mb}} B_{i;z^+}, \quad i = 2, \ldots, N, \tag{8}$$

where k_{mb} is the attachment rate. This reaction accounts for interactions between activated monomers and the bundles and attachment of the former to the latter.

A graphical representation of reactions in Eqs. 1–8 is depicted in Fig. 1. ODEs for each of the reactions in Eqs. 1–8 are provided in Section S1.

Following other multifilament models, e.g., Lan et al. (56), Frieden and Goddette (58), Sept et al. (59), and Falzone et al. (60), we use the conservation of mass to estimate the average length of filaments and bundles, $\overline{L}^m_{fb}$. At any time, the total concentration of monomers, C_{tot}, is the sum of the concentration of nonactivated and activated monomers, $[Z^{na}]$ and $[Z]$, and the cumulative concentrations of monomers in different forms, e.g., twice the concentration of dimers, three times the concentration of trimers, etc. Because the length of filaments is a multiple of the monomers, this yields

$$C_{tot} = [Z^{na}] + [Z] + \sum_{i=2}^{6} i[Z_i] + \overline{L}^m_{fb}\left([F] + \sum_{i=2}^{N} i[B_i]\right)$$

or

$$\overline{L}^m_{fb} = \frac{C_{tot} - [Z^{na}] - [Z] - \sum_{i=2}^{6} i[Z_i]}{[F] + \sum_{i=2}^{N} i[B_i]}. \tag{9}$$

This quantity keeps track of the average number of monomers, hence the superscript m, longitudinally connected per filament/bundle during the entire assembly process. The smallest length of a filament is $\overline{L}^m_{fb} = 7$, i.e., a filament consists of seven monomers. This value is achieved instantaneously once $[F]$ becomes larger than zero. To avoid having to deal with this jump discontinuity in time, we define an average total length, $\overline{L}^m_{tot}$, which includes the first oligomers (Z_2,…, Z_6),

$$\overline{L}^m_{tot} = \frac{\sum_{i=2}^{6} i[Z_i] + \overline{L}^m_{fb}\left([F] + \sum_{i=2}^{N} i[B_i]\right)}{\sum_{i=2}^{6} [Z_i] + [F] + \sum_{i=2}^{N} i[B_i]}. \tag{10}$$

This parameter gives a complete description of the average length of filaments in all forms (short oligomers and longer filaments) and bundles. The average characteristics $\overline{L}^m_{fb}$ and $\overline{L}^m_{tot}$ play a crucial role in reducing the number of species and, therefore, the number of equations used to describe the protein assembly process. In Section S2, we demonstrate that the definition of the average length in Eq. 9 enforces mass conservation. Energy is also conserved, but the principle of microscopic reversibility, or detailed balance, is violated (see Section S2 for more detail).

Another important characteristic of the polymerization process is the average width of a bundle, $\overline{W}^f_{tot}$, or the average number of filaments per bundle. It is defined as

$$\overline{W}^f_{tot} = \frac{\sum_{i=2}^{6} i[Z_i] + \overline{L}^m_{fb}\left([F] + \sum_{i=2}^{N} i[B_i]\right)}{\sum_{i=2}^{6} i[Z_i] + \overline{L}^m_{fb}\left([F] + \sum_{i=2}^{N} [B_i]\right)}, \tag{11}$$

where the species Z_2,…, Z_6, and F are treated as bundles of an average width 1.

Our model does not account for the "cozy corner association" (46), which allows for simultaneous formation of longitudinal and lateral bonds and acts as a sliding mechanism between polymers. This omission is informed by the recent experimental study (41) that indicates that filaments in a bundle network do not slide but, rather, exhibit a treadmill-like behavior.

Models 1–10 consist of a system of 17 ODEs. This system was solved with an ODE45 MATLAB function (The MathWorks, Natick, MA), which implements a combination of fourth- and fifth-order Runge-Kutta methods for nonstiff differential equations.

Model parameterization

We use the in vitro study (22) of FtsZ-F268C polymerization in MMK buffer to parameterize our model, i.e., to determine values of the reaction rates in Eqs. 1–8. We focus on this strain because it is an innocuous mutation that shows identical assembly to the wild-type FtsZ (22,23,41,49). Unlike wild-type FtsZ, the mutant F268C has a single cysteine that provides a mechanism to attach the fluorescent labels and facilitates the assembly assay based on fluorescence resonance energy transfer. The experiments of Chen and Erickson (22) cover a wide range of FtsZ concentrations, from the critical concentration to polymerize (0.7 μM for this experiment) to the 5–10 μM representative of in vivo conditions (56,62,63), and their findings are in agreement with other investigations. These findings include the average filament length of 100–200 nm, also observed in Dajkovic et al. (53), Popp et al. (55), and Romberg et al. (64); the average bundle width of 5–15 nm, as seen in Chen and Erickson (23), Dajkovic et al. (53), Huecas et al. (54), and Romberg et al. (64); and the monomer turnover rate of 0.143 s^{-1}, which falls within the range of 0.112–0.233 s^{-1} observed in in vitro experiments (41,52,65) and is close to in vivo values of 0.111–0.128 s^{-1} (18).

Values of the reaction rates and other model parameters are summarized in Table 2. Most of them are taken from the literature, while the remaining

TABLE 2 Reaction Rates and Bond Energies

Parameter	Units	Value	Reference
k_{ac}^{+}	s^{-1}	0.38	(22)
k_{ac}^{-}	s^{-1}	0.01	(22)
k_{nu}^{+}	$\mu M^{-1}\ s^{-1}$	0.79	(22)
k_{nu}^{-}	s^{-1}	199.8	(22)
k_{el}^{+}	$\mu M^{-1}\ s^{-1}$	6.6	(22)
k_{an}^{+}	$\mu M^{-1}\ s^{-1}$	6.6	(22)
k_{bu}^{+}	$\mu M^{-1}\ s^{-1}$	3.5981	calibrated
k_{bu}^{0}	s^{-1}	199.8221	calibrated
k_{mb}	$\mu M^{-1}\ s^{-1}$	2.7288	calibrated
$k_{hss/dis}^{1}$	s^{-1}	0.6681	calibrated
$k_{hss/dis}^{2}$	s^{-1}	0.143	(22)
$k_{hss/dis}^{3}$	s^{-1}	0.112	(41)
ΔU_t	k_BT[a]	4.05	(22,56)
ΔU_m	k_BT[a]	8.10	(56)
U_b	k_BT[a]	0.175	(53,56)[b]

[a]The energy units are expressed in terms of the Boltzmann constant k_B and room temperature T.
[b]Simple bundling model.

four are estimated in Section S3 by calibrating our model to the low steady-state concentration data ($C_{tot} = 0.7$–$3.0\ \mu M$) from Chen and Erickson (22). The low concentration data at short and long times are used in Section S4 for model validation.

The values of the activation and nucleation reaction rates in Eqs. 1 and 2 are taken from the model in Chen and Erickson (22). Following Chen and Erickson (22) and Frieden and Goddette (58), we both assume the forward (k_{el}^{+}) and backward (k_{el}^{-}) reaction rates in Eq. 3 to be independent of a filament's length (i.e., to be the same for all i) and set $k_{-7} = 0$. By treating the reaction in Eq. 3b as irreversible, the latter step allows one to avoid a buildup of Z_6 polymers as the concentration of filaments F increases, and ensures that the reaction rate values do not change when the number of elongation steps increases beyond seven (22).

While elongation and annealing in Eq. 4 are diffusion-limited reactions, we treat them as reaction-limited because of the small average size of the FtsZ polymers observed in the experiments. Previous models (45,56,57) assume that rates for elongation and annealing are equal and independent of the filament length, i.e., $k_{el}^{+} = k_{ann}^{+} =$ constant. Although the authors of Lan et al. (56) explicitly mention the diffusion-limited character of these reactions, they do not explain why the rates do not decrease as the filaments get longer; and the model in Erickson (46) does the same for bundling reactions. We justify this choice by proposing an analogy between models of FtsZ filament growth and actin assembly. (For long filaments ($\overline{L}_{actin} \geq 100$ monomers), the annealing reaction rate of actin polymerization, $k_{ann,\,actin}^{+}$, decreases with the average length (59,66,67). For shorter filaments ($\overline{L}_{actin} = 65$ monomers), $k_{ann,\,actin}^{+}$ is considered constant and smaller than the elongation rate $k_{el,\,actin}^{+}$ (68). For small filaments ($\overline{L}_{actin} < 30$ monomers), the two rates are considered constant and similar, $k_{ann,\,actin}^{+} \approx k_{el,\,actin}^{+} \approx 10\ \mu M\ s^{-1}$ (69).) Because the longest average length of FtsZ filaments in our model is $\overline{L}_{tot}^{m} \approx 30$ monomers, this analogy suggests $k_{el}^{+} = k_{ann}^{+} =$ constant.

For the concentrations reported in Chen and Erickson (22), the bundling reaction rates in Eq. 5 are limited by the size of a filament bundling to either another filament or a bundle. Therefore, the bundling rate k_{bu}^{+} should be close to the annealing rate k_{ann}^{+}, and its value must fall within the accepted range of protein-protein association rates, 2.0–7.5 $\mu M^{-1}\ s^{-1}$ (22,41,70). The parameter identification procedure described in Section S3 honors this constraint.

The depolymerization reaction rates, k_{el}^{-}, k_{an}^{-}, and k_{bu}^{-}, are determined from the respective internal energies of filaments and bundles. Specifically, the backward reaction rates for elongation and annealing are given by (56)

$$k_{el}^{-} = k_{nu}^{-}\, e^{-\Delta U_t} \quad \text{and} \quad k_{an}^{-} = k_{nu}^{-}\, e^{-\Delta U_m}, \tag{12}$$

where ΔU_t and ΔU_m are the increments in the energy of a monomer connected at the end and middle of a filament, respectively. The value of ΔU_t is calculated from the first expression in Eq. 12, with the values for k_{nu}^{-} and k_{el}^{-} taken from Chen and Erickson (22). Conservation of energy suggests (56) that $\Delta U_m = 2\Delta U_t$. The lateral dissociation rate k_{bu}^{-} decreases exponentially with the average length of the connected filaments/bundles (56),

$$k_{bu}^{-} = \begin{cases} k_{bu}^{0} & \overline{L}_{fb}^{m} \leq 1, \\ k_{bu}^{0}\, e^{-\left(\overline{L}_{fb}^{m}-1\right)U_b} & \overline{L}_{fb}^{m} > 1, \end{cases} \tag{13}$$

where U_b is the bond energy per lateral bond. Its value of $U_b = 0.175\ k_BT$ represents both the average of the values reported in Dajkovic et al. (53) for the same strain as in Chen and Erickson (22) but a different buffer, and the value used in Lan et al. (56) for a strain different from Chen and Erickson (22) but for the same buffer. The reference dissociation rate k_{bu}^{0} is one of the four parameters used for model calibration. In the absence of experimental evidence, we have explored a wide range of values (0.0–500 s^{-1}) in the calibration procedure described in Section S3.

Dissociation of monomers after GTP hydrolysis is essentially absent in the beginning of polymerization (22,52); it becomes more pronounced as the amount of polymers increases and they interact more frequently with GDP. This dependence of the hydrolysis/dissociation rates in Eqs. 6 and 7 on the amount of polymers is accounted for as

$$k_{hy/dis}^{i} = k_{hss/dis}^{i} \frac{C_{tot} - [Z^{na}] - [Z]}{C_{tot} - C_{cr}^{1}}, \quad i = 1, 2, 3, \tag{14}$$

where $C_{cr}^{1} < C_{tot}$ in the second regime of polymerization. At the beginning of the assembly process, most FtsZ proteins are in the form of nonactivated (Z^{na}) and activated (Z) monomers, such that $[Z^{na}] + [Z] \approx C_{tot}$ and $k_{hy/dis}^{i} \to 0$. At steady state, when the polymer network is formed and GDP deactivates monomers more often, these rates reach their maximum values, $k_{hy/dis}^{i} \approx k_{hss/dis}^{i}$ for $i = 1, 2, 3$. They represent the rate with which a GTP-bound monomer in a filament or a bundle changes its nucleotide and leaves the filament bounded to GDP, i.e., the turnover rate predominantly associated with GTP hydrolysis.

The reaction rates controlling dissociation after GTP hydrolysis depend on the location of a deactivated monomer in the filament or bundle. In Table 2, $k_{hss/dis}^{i}$ ($i = 1, 2, 3$) denote values of the hydrolysis rates for filaments and bundles at steady state. Only the rate for detachment of monomers from filament ends, $k_{hss/dis}^{1}$, was calibrated. The rate for detachment of monomers from the middle of filaments and thin bundles, $k_{hss/dis}^{2}$, is set to the average value reported in Chen and Erickson (22) for turnover of monomers at steady state (half-time of 7 s, i.e., 0.143 s^{-1}), because we assume that it is the depolymerization reaction that happens more often. This assumption is based on two facts: the predominant species observed in the experiment are filaments and thin bundles; and there are more monomers in the middle of filaments and bundles than in their ends. The value of $k_{hss/dis}^{3}$ is determined in Arumugam et al. (41) by observing the detachment of nonactivated monomers from thick bundles. These three rates satisfy the following order relations. It takes less energy to break a longitudinal bond at the filament end than two bonds at its middle, therefore, $k_{hss/dis}^{1} > k_{hss/dis}^{2}$ (61) (the condition imposed for calibration of $k_{hss/dis}^{1}$ in Section S3). The values of $k_{hss/dis}^{2}$ for shortening of filaments and thin bundles are equal, because both reactions describe the loss of a monomer in the middle of a filament. The value of $k_{hss/dis}^{3}$ is the smallest of the three rates, because the monomers in a bundle can be doubly connected both longitudinally and laterally.

The rate at which activated monomers in the solution attach themselves to bundles, a process represented by Eq. 8, is quantified by the reaction rate constant k_{mb}. The latter serves as the final calibration parameter; its computed value (Table 2) is imposed to fall within the range of values of the protein-protein interaction rates of 2–7.5 $\mu M^{-1}\ s^{-1}$. The condition

$k_{mb} < k_{el}^{+} = 6.6\ \mu M^{-1}\ s^{-1}$ is also imposed (see Section S3), because pure longitudinal attachments of monomers to filament ends are more favorable than combinations of both longitudinal and lateral attachments in a monomer-bundle interaction.

RESULTS AND DISCUSSION

Results of model calibration and validation on the low concentration data from Chen and Erickson (22), C_{tot} = 0.7–3.0 μM, are presented in Sections S3 and S4, respectively. In what follows, we present fit-free predictions for high concentrations of C_{tot} = 3.0–10.0 μM (Model Predictions at High Concentrations, C_{tot} = 3.0–10.0 μM); discuss what are, to our knowledge, new insights provided by our model (Physiological Insights); and compare its performance with that of its counterparts (Comparison with Alternative Models). The steady-state data at high concentrations (C_{tot} = 3.0–10.0 μM) are taken from Chen and Erickson (22) and used to validate our model.

Model predictions at high concentrations, C_{tot} = 3.0–10.0 μM

Average size of the filaments and bundles

Under physiologically relevant conditions, C_{tot} = 5.0–10.0 μM, our model captures the observed tendency of the filaments to keep the same average length $\overline{L}_{tot}^{m} \approx 32 - 33$ subunits at steady state, regardless of the value of C_{tot} (Fig. 3). Tables 3 and S4 show that, for C_{tot} = 2.0–10.0 μM, the predicted average length is $\overline{L}_{tot}^{m} = 25 - 33$ subunits (125–165 nm), which is within the well-established range of 100–200 nm (46,50,53–55,64).

Almost all filaments remain single-stranded when $C_{tot} <$ 2.0 μM (Table S4). For larger concentrations up to C_{tot} = 10.0 μM, and for various buffers and FtsZ strains, filaments dominate and the majority of bundles consist of two filaments. All the computed values of the average bundle width $\overline{W}_{tot}^{f}$ in Table 3 (and Fig. 3) are <2, which is in agreement not only with Chen and Erickson (22) but also with other experiments (23,53,54,64).

Concentration of monomers at steady state

In the physiologically relevant range of C_{tot} = 5.0–10.0 μM, our model predicts the steady-state concentration of monomers to be $[Z^{na}]_{ss} + [Z]_{ss} \approx 0.7\ \mu M$ (Table 3). This matches the observed monomer concentration (22) and equals the first critical concentration, C_{cr}^{1}. The model presented in Chen and Erickson (22) underestimates this observation, predicting a value of $[Z^{na}]_{ss} + [Z]_{ss} \approx 0.5\ \mu M$.

Physiological insights

Second critical concentration

An appreciable decrease in the fluorescence intensity at C_{tot} = 3.0 μM (or, more generally, at C_{tot} = 2.0–4.0 μM, depending on the concentration of Mg^{2+} contained in the buffer) was observed, but not explained, by Chen and Erickson (22). A subsequent kinetics model in Lan et al. (56) utilized the experimental data from Chen et al. (50) and Chen and Erickson (22) to describe this phenomenon by identifying a critical concentration, C_{cr}^{2}, at which the presence of bundles becomes pronounced. The model in Lan et al. (56) does not specify the value of C_{cr}^{2} and, crucially, predicts formation of bundles comprising two or three filaments at low concentrations (C_{tot} = 2.0 μM), which is not supported by the observations. Our model correctly predicts the average length/width for filaments and bundles for a range of C_{tot}. This ratio reaches its maximum at C_{tot} = 2.5 μM, the critical concentration C_{cr}^{2} after which the longitudinal growth (elongation and/or annealing) ceases to dominate the lateral growth (bundling) and bundles become an important factor in the overall kinetics (Fig. 4). Our predicted value of C_{cr}^{2} = 2.5 μM falls within the experimentally observed range of 2–4 μM. We posit that the maximum average length/width corresponds

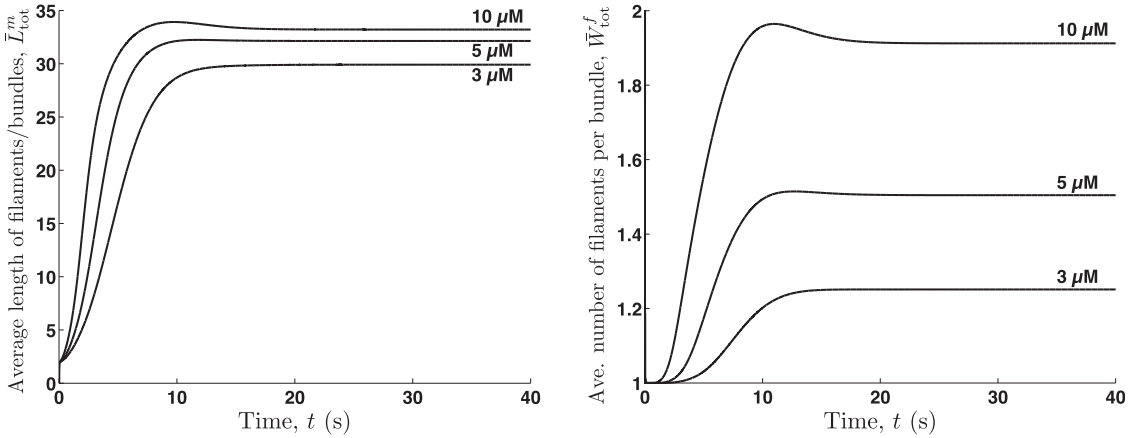

FIGURE 3 Temporal evolution of the average number of monomers connected longitudinally into filaments and bundles (*left*) and the average number of filaments per bundle (*right*), for C_{tot} = 3.0, 5.0, and 10.0 μM.

TABLE 3 Steady-State Monomer Concentration and Average Length and Width Predicted with Our Model and Observed in Experiments (22)

Concentration	Average Length: $\overline{L}^m_{tot}$		Average Width: $\overline{W}^f_{tot}$		Monomer Concentration: $[Z^{na}]_{ss} + [Z]_{ss}(\mu M)$		
C_{tot} (μM)	Predicted	Observed	Predicted	Observed	Predicted	Observed	Model (22)
4.0	31.42	30	1.39	<2	0.693	0.7	0.537
5.0	32.14	30	1.50	<2	0.691	0.7	0.538
6.0	32.55	30	1.60	<2	0.690	0.7	0.538
7.0	32.81	30	1.69	<2	0.690	0.7	0.539
8.0	32.99	30	1.77	<2	0.689	0.7	0.539
9.0	33.12	30	1.84	<2	0.689	0.7	0.539
10.0	33.21	30	1.91	<2	0.690	0.7	0.539

to the transition between a network formed entirely by filaments and a thicker network made of both filaments and bundles.

Role of bundling in dissociation of monomers after hydrolysis

Because the average length $\overline{L}^m_{tot}$ remains nearly constant for $C_{tot} > 3.0$ μM or 29–33 subunits (Table 3), this characteristic length is probably sufficient for formation of stable bundles. The bundling regulates turnover of monomers keeping GTP-hydrolysis/dissociation rate constant for concentrations $C_{tot} = 3.0$–10.0 μM, at which bundles become relevant (22). That regulation also helps to maintain the average length of the filaments constant and to keep the system at this equilibrium state regardless of the total concentration. Because this occurs at in vivo concentrations levels, $C_{tot} = 3.0$–10.0 μM, we posit that the interaction of bundle formation and GTP hydrolysis is a key part of the FtsZ ring formation and steady-state equilibrium until contraction.

Limitations of fluorescence resonance energy transfer assay for measurements related to bundling

The existence of the second critical concentration related to bundling, C^2_{cr}, highlights a potential limitation of the fluorescence resonance energy transfer assay used in Chen and Erickson (22). The authors reported the fluorescence intensities, which serve as proxy for the amount of FtsZ in filaments and bundles, to be lower than expected. Accounting for the exchange of monomers between solution and bundles (see Eqs. 7b and 8) provides an explanation for this phenomenon. These reactions cause the bundles to continuously lose and gain monomers even at steady state, which generates bundles partially connected longitudinally; this exchange can be described with a stochastic model (41). This longitudinal elongation of the bundles distorts the measured fluorescence intensities, because the fluorescence resonance energy transfer assay signals are direct measurements of the longitudinal contacts of FtsZ species.

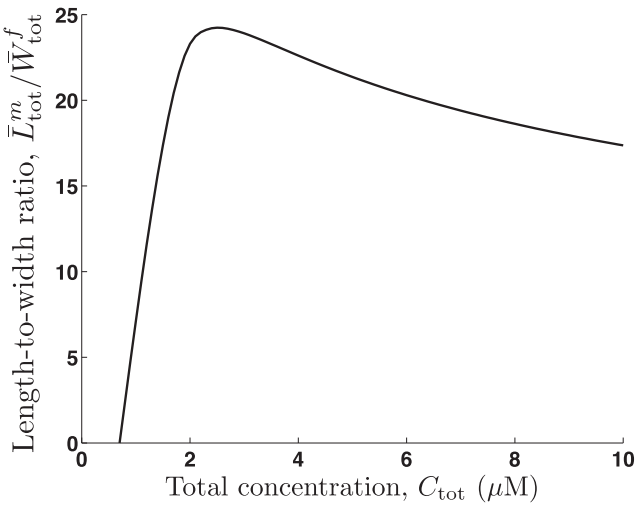

FIGURE 4 Length/width for the filaments and bundles at steady state, for a range of concentration C_{tot}.

Comparison with alternative models

Borrowing from Chen and Erickson (23), our model accounts for the following aspects of FtsZ assembly: reversible exchange of monomers bounded to GTP at the end of filaments (Eq. 3c), irreversible annealing (forward reaction in Eq. 4), and the loss of monomers bounded to GDP at the ends (Eq. 6a) and middle of filaments (Eq. 6b) after GTP hydrolysis. Our model departs from Chen and Erickson (23) by introducing a reversible annealing (Eq. 4), because fragmentation of a filament in the middle can be due to the separation of two monomers bounded to GTP (64). Crucially, our model includes a description of the depolymerization process by including reactions for bundles (Eqs. 7a and 7b).

The predictive power of our model, which consists of 17 ODEs, compares favorably with that of its more complex alternatives, which comprise hundreds or thousands of ODEs (see Table 1). Our model's development was motivated by the three models of increasing complexity introduced by Lan et al. (56). The simplest, single-filament model (denoted by M1 in Table 1) captures the kinetics of FtsZ assembly at low FtsZ concentrations, $C_{tot} \leq 2.0$–3.0 μM. Even though it employs 500 ODEs to determine the steady-state length distribution of filaments, it does not account for filament bundling and is discarded by the authors in favor of the more complex alternatives. By allowing formation of two-filament bundles, the second of these models (denoted by M2 in Table 1, and comprising

500 ODEs) improves the predictive accuracy of polymer length distribution at low concentrations ($C_{tot} = 2.0\ \mu M$). Yet, model M2 significantly overestimates the length of bundles at high concentrations ($C_{tot} = 10.0\ \mu M$).

The third model in Lan et al. (56) consists of 1254 ODEs and, similar to our model, computes an average length of filaments and bundles rather than a complete distribution of their lengths. It has been rejected by the authors because of its complexity and apparent inability to correctly predict the experimentally observed average length of filaments and bundles and the average width of bundles. Specifically, this model predicts the average length $\overline{L}_{tot}$ to be 300 nm instead of the experimentally observed value of ~120 nm (22). Rather than attributing this overestimation to the deficiency of the modeling approach, i.e., the reliance on the average length, we believe it to stem both from an inappropriate choice of the value for reaction rate k_{nu}^{-} and from the oversimplified representation of dissociation of monomers after GTP hydrolysis. Likewise, their model overestimates the width of the bundles: it predicts an average of two or three filaments per bundle for $C_{tot} = 2.0\ \mu M$, while the experiment (22) found almost all filaments to be single-stranded. We attribute this discrepancy to an inappropriate selection of values of the reaction rates k_{bu}^{+} and k_{bu}^{0}, and to the overestimation of the average length ($\overline{L}_{tot} \approx 300$ nm). According to Eq. 13, the latter leads to an underestimation of the lateral dissociation rate of filaments/bundles k_{bu}^{-}.

The model of Surovtsev et al. (57) and its subsequent generalization (45) handle a distribution of polymer lengths (rather than their average) and explicitly account for hydrolysis reactions at both the ends and middle of a filament. While these models assume that these two reactions have the same rate, our model assigns a higher rate for GDP-bound monomer dissociation from the end of a filament after hydrolysis than from the middle, as observed experimentally in Mateos-Gil et al. (61). Consequently, our model makes better predictions for dissociation after hydrolysis than Surovtsev et al. (57) (they estimated concentration of monomers at the steady state 2–10 times lower than in vitro experimental values). Moreover, the models in Dow et al. (45) and Surovtsev et al. (57) consist of ~300 ODEs and ignore filament bundling. The latter implies that they predict neither a bundle size nor the critical concentration at which bundles become pronounced. Finally, these models fail to identify the strong dependence between dissociation of monomers after GTP hydrolysis and bundle formation (41,52,64).

CONCLUSIONS

We developed a computationally efficient model of protein polymerization, which relies on an average length of polymers (rather than on length distribution) to significantly reduce the number of reaction rate equations. Our model of FtsZ assembly in *E. coli*, a phenomenon used as an illustrative example, consists of 17 ODEs and equals or exceeds the predictive power of its alternatives (45,56,57), which comprise hundreds or thousands of ODEs. The simplicity and, hence, computability of our model are essential elements for its use as a component in simulations of an *E. coli* cell lifecycle, which in addition to FtsZ assembly also includes attachment/detachment to/from the cell membrane, polymerization inhibition by MinCD and SlmA proteins, formation of bundles and clusters by other proteins, etc.

It is often argued, e.g., by Lan et al. (56), that reducing the number of species (and, hence, ODEs) by defining an average concentration of filaments (and their average length) leads to significant model errors. We demonstrated that an improved kinetic description of the FtsZ assembly process yields more accurate and computationally efficient predictions than those obtained with the multifilament model (56).

Despite its relative simplicity, our model captures key aspects of depolymerization after GTP hydrolysis and filament bundling in cytoskeletal structures in a way that its more complex counterparts do not. FtsZ filaments in *E. coli* bundle by lateral bonds or through the action of other proteins like ZapA or ZapB. Our model reproduces the experimental finding (53,56) that lateral interactions between FtsZ monomers or small filaments are weak. It also shows that, as filaments grow longitudinally, bundling becomes essential for the stability and robustness of the scaffold. In the physiologically relevant conditions of the total monomer concentration $C_{tot} = 5.0–10.0\ \mu M$, once the filaments grow to the length of ~30 subunits, they start forming bundles. Our model reproduces, both qualitatively and quantitatively, this phenomenon as well as the FtsZ polymerization at low concentrations ($C_{tot} \leq 2.0\ \mu M$), observed in Chen and Erickson (22).

Because our model describes protein assembly in terms of elementary (and bimolecular) reactions only, it is readily amenable to stochastic simulations that replace continuum reaction rate ODEs with their discrete counterparts, e.g., Choi et al. (71). Our model is directly applicable to homogeneous systems, such as in vitro experiments in which the entire process of protein assembly occurs in well-mixed solutions without spatial preferences to polymerize. It can be generalized to account for the presence of concentration gradients either by adding diffusion terms to the ODEs or by employing stochastic operator-splitting algorithms, e.g., Choi et al. (72).

Another approach to dealing with spatial heterogeneity ubiquitous in in vivo systems is to partition a cell into homogeneous compartments. In the context of bacterial cell division, such compartments are cell caps and a midcell region (45). FtsZ filaments and bundles in the cell caps are shorter and thinner than in the midsection, because of the action of MinCD and SlmA proteins that continuously extract monomers from the FtsZ network (43,73,74).

Deploying our model in each of the three homogeneous compartments and using Fick's law to compute fluxes of FtsZ species between any two adjacent components would yield a spatially varying average length of filaments and bundles.

Our reduced-order representation of reactions, such as bundling or turnover of subunits as a consequence of hydrolysis, facilitates its adoption to other cytoskeletal biopolymers. Apart from elongation and annealing, the formation of bundles with and without intervention of other proteins is a characteristic process in network assembly of actin filaments (by fimbrin or α-actinin), microtubules (by MAP2) and intermediate filaments in eukaryotes, or MreB (by YeeU) and ParM in prokaryotes (60,75,76). Our FtsZ model can be modified to define the characteristic net cycle balance of other cytoskeletal filaments (77–79) in terms of simple reactions. Polymerization/depolymerization processes regulated by the action of nucleotides, such as ATP/ADP or GTP/GDP, are also common in cytoskeleton formation. Our model already includes reactions of this nature, but it can be improved by defining nucleotides as a new species and describing more explicitly their interactions with biopolymers. We leave these and other enhancements of our model for future studies.

SUPPORTING MATERIAL

Supporting Materials and Methods, four figures, and four tables are available at http://www.biophysj.org/biophysj/supplemental/S0006-3495(16)30331-9.

AUTHOR CONTRIBUTIONS

A.R.-M. performed research and wrote the article; T.M.B., T.J.S., and D.M.T. designed research and wrote the article; and all authors agree on the content of the article.

ACKNOWLEDGMENTS

This work was supported in part by the Howard Hughes Medical Institute, the National Institutes of Health under grant No. MH079076, the Salk Innovation Award, the Defense Advanced Research Projects Agency under the EQUiPS program, the Air Force Office of Scientific Research under grant No. FA9550-12-1-0185, and the National Science Foundation under grant No. DMS-1522799.

SUPPORTING CITATIONS

References (80–82) appear in the Supporting Material

REFERENCES

1. Wickstead, B., and K. Gull. 2011. The evolution of the cytoskeleton. *J. Cell Biol.* 194:513–525.
2. Ingerson-Mahar, M., and Z. Gitai. 2012. A growing family: the expanding universe of the bacterial cytoskeleton. *FEMS Microbiol. Rev.* 36:256–266.
3. Xu, K., H. P. Babcock, and X. Zhuang. 2012. Dual-objective STORM reveals three-dimensional filament organization in the actin cytoskeleton. *Nat. Methods.* 9:185–188.
4. Yi, K., and R. Li. 2012. Actin cytoskeleton in cell polarity and asymmetric division during mouse oocyte maturation. *Cytoskeleton (Hoboken).* 69:727–737.
5. Fischer, R. S., and V. M. Fowler. 2015. Thematic minireview series: the state of the cytoskeleton in 2015. *J. Biol. Chem.* 290:17133–17136.
6. Bathe, M., C. Heussinger, …, E. Frey. 2008. Cytoskeletal bundle mechanics. *Biophys. J.* 94:2955–2964.
7. Lutkenhaus, J., S. Pichoff, and S. Du. 2012. Bacterial cytokinesis: from Z ring to divisome. *Cytoskeleton (Hoboken).* 69:778–790.
8. Dixon, R. D., D. K. Arneman, …, C. A. Otey. 2008. Palladin is an actin cross-linking protein that uses immunoglobulin-like domains to bind filamentous actin. *J. Biol. Chem.* 283:6222–6231.
9. Erb, M. L., J. A. Kraemer, …, J. Pogliano. 2014. A bacteriophage tubulin harnesses dynamic instability to center DNA in infected cells. *eLife.* 3:6222–6231.
10. Walczak, C. E., and S. L. Shaw. 2010. A MAP for bundling microtubules. *Cell.* 142:364–367.
11. Stevenson, R. P., D. Veltman, and L. M. Machesky. 2012. Actin-bundling proteins in cancer progression at a glance. *J. Cell Sci.* 125:1073–1079.
12. Mattila, P. K., and P. Lappalainen. 2008. Filopodia: molecular architecture and cellular functions. *Nat. Rev. Mol. Cell Biol.* 9:446–454.
13. Koskinen, M., and P. Hotulainen. 2014. Measuring F-actin properties in dendritic spines. *Front. Neuroanat.* 8:74.
14. Medeiros, N. A., D. T. Burnette, and P. Forscher. 2006. Myosin II functions in actin-bundle turnover in neuronal growth cones. *Nat. Cell Biol.* 8:215–226.
15. Penzes, P., and I. Rafalovich. 2012. Regulation of the actin cytoskeleton in dendritic spines. *Adv. Exp. Med. Biol.* 970:81–95.
16. Salje, J., B. Zuber, and J. Löwe. 2009. Electron cryomicroscopy of *E. coli* reveals filament bundles involved in plasmid DNA segregation. *Science.* 323:509–512.
17. Nurse, P., and K. J. Marians. 2013. Purification and characterization of *Escherichia coli* MreB protein. *J. Biol. Chem.* 288:3469–3475.
18. Anderson, D. E., F. J. Gueiros-Filho, and H. P. Erickson. 2004. Assembly dynamics of FtsZ rings in *Bacillus subtilis* and *Escherichia coli* and effects of FtsZ-regulating proteins. *J. Bacteriol.* 186:5775–5781.
19. Li, Z., M. J. Trimble, …, G. J. Jensen. 2007. The structure of FtsZ filaments in vivo suggests a force-generating role in cell division. *EMBO J.* 26:4694–4708.
20. Fu, G., T. Huang, …, J. Xiao. 2010. In vivo structure of the *E. coli* FtsZ-ring revealed by photoactivated localization microscopy (PALM). *PLoS One.* 5:e12682.
21. Srinivasan, R., M. Mishra, …, M. K. Balasubramanian. 2007. Filament formation of the *Escherichia coli* actin-related protein, MreB, in fission yeast. *Curr. Biol.* 17:266–272.
22. Chen, Y., and H. P. Erickson. 2005. Rapid in vitro assembly dynamics and subunit turnover of FtsZ demonstrated by fluorescence resonance energy transfer. *J. Biol. Chem.* 280:22549–22554.
23. Chen, Y., and H. P. Erickson. 2009. FtsZ filament dynamics at steady state: subunit exchange with and without nucleotide hydrolysis. *Biochemistry.* 48:6664–6673.
24. Rottner, K., and T. E. B. Stradal. 2011. Actin dynamics and turnover in cell motility. *Curr. Opin. Cell Biol.* 23:569–578.
25. Hernández-Rocamora, V. M., B. Reija, …, M. Vicente. 2010. Dynamic interaction of the *Escherichia coli* cell division ZipA and FtsZ proteins evidenced in nanodiscs. *J. Biol. Chem.* 36:30097–30104.
26. Pichoff, S., and J. Lutkenhaus. 2005. Tethering the Z ring to the membrane through a conserved membrane targeting sequence in FtsA. *Mol. Microbiol.* 55:1722–1734.

27. Rowlett, V. W., and W. Margolin. 2014. 3D-SIM super-resolution of FtsZ and its membrane tethers in *Escherichia coli* cells. *Biophys. J.* 107:L17–L20.

28. Loose, M., and T. J. Mitchison. 2014. The bacterial cell division proteins FtsA and FtsZ self-organize into dynamic cytoskeletal patterns. *Nat. Cell Biol.* 16:38–46.

29. Mohammadi, T., G. E. J. Ploeger, …, T. den Blaauwen. 2009. The GTPase activity of *Escherichia coli* FtsZ determines the magnitude of the FtsZ polymer bundling by ZapA in vitro. *Biochemistry.* 48:11056–11066.

30. Buss, J., C. Coltharp, …, J. Xiao. 2013. In vivo organization of the FtsZ-ring by ZapA and ZapB revealed by quantitative super-resolution microscopy. *Mol. Microbiol.* 89:1099–1120.

31. Dajkovic, A., S. Pichoff, …, D. Wirtz. 2010. Cross-linking FtsZ polymers into coherent Z rings. *Mol. Microbiol.* 78:651–668.

32. Mercier, R., M.-A. Petit, …, O. Espéli. 2008. The MatP/matS site-specific system organizes the terminus region of the *E. coli* chromosome into a macrodomain. *Cell.* 135:475–485.

33. Bailey, M. W., P. Bisicchia, …, J. Männik. 2014. Evidence for divisome localization mechanisms independent of the Min system and SlmA in *Escherichia coli*. *PLoS Genet.* 10:e1004504.

34. Männik, J., and M. W. Bailey. 2015. Spatial coordination between chromosomes and cell division proteins in *Escherichia coli*. *Front. Microbiol.* 6:306.

35. Huang, K. C., Y. Meir, and N. S. Wingreen. 2003. Dynamic structures in *Escherichia coli*: spontaneous formation of MinE rings and MinD polar zones. *Proc. Natl. Acad. Sci. USA.* 100:12724–12728.

36. Meinhardt, H., and P. A. J. de Boer. 2001. Pattern formation in *Escherichia coli*: a model for the pole-to-pole oscillations of Min proteins and the localization of the division site. *Proc. Natl. Acad. Sci. USA.* 98:14202–14207.

37. Kerr, R. A., H. Levine, …, W.-J. Rappel. 2006. Division accuracy in a stochastic model of Min oscillations in *Escherichia coli*. *Proc. Natl. Acad. Sci. USA.* 103:347–352.

38. Cho, H., H. R. McManus, …, T. G. Bernhardt. 2011. Nucleoid occlusion factor SlmA is a DNA-activated FtsZ polymerization antagonist. *Proc. Natl. Acad. Sci. USA.* 108:3773–3778.

39. Tonthat, N. K., S. L. Milam, …, M. A. Schumacher. 2013. SlmA forms a higher-order structure on DNA that inhibits cytokinetic Z-ring formation over the nucleoid. *Proc. Natl. Acad. Sci. USA.* 110:10586–10591.

40. Shen, B., and J. Lutkenhaus. 2010. Examination of the interaction between FtsZ and MinCN in *E. coli* suggests how MinC disrupts Z rings. *Mol. Microbiol.* 75:1285–1298.

41. Arumugam, S., Z. Petrašek, and P. Schwille. 2014. MinCDE exploits the dynamic nature of FtsZ filaments for its spatial regulation. *Proc. Natl. Acad. Sci. USA.* 111:E1192–E1200.

42. Shen, B., and J. Lutkenhaus. 2009. The conserved C-terminal tail of FtsZ is required for the septal localization and division inhibitory activity of MinC(C)/MinD. *Mol. Microbiol.* 72:410–424.

43. Du, S., and J. Lutkenhaus. 2014. SlmA antagonism of FtsZ assembly employs a two-pronged mechanism like MinCD. *PLoS Genet.* 10:e1004460.

44. Tsukanov, R., G. Reshes, …, M. Feingold. 2011. Timing of Z-ring localization in *Escherichia coli*. *Phys. Biol.* 8:066003.

45. Dow, C. E., A. Rodger, …, H. A. van den Berg. 2013. A model of membrane contraction predicting initiation and completion of bacterial cell division. *Integr. Biol. (Camb.).* 5:778–795.

46. Erickson, H. P. 2009. Modeling the physics of FtsZ assembly and force generation. *Proc. Natl. Acad. Sci. USA.* 106:9238–9243.

47. Lan, G., C. W. Wolgemuth, and S. X. Sun. 2007. Z-ring force and cell shape during division in rod-like bacteria. *Proc. Natl. Acad. Sci. USA.* 104:16110–16115.

48. Turner, D. J., I. Portman, …, M. S. Turner. 2012. The mechanics of FtsZ fibers. *Biophys. J.* 102:731–738.

49. Arumugam, S., G. Chwastek, …, P. Schwille. 2012. Surface topology engineering of membranes for the mechanical investigation of the tubulin homologue FtsZ. *Angew. Chem. Int. Ed. Engl.* 51:11858–11862.

50. Chen, Y., K. Bjornson, …, H. P. Erickson. 2005. A rapid fluorescence assay for FtsZ assembly indicates cooperative assembly with a dimer nucleus. *Biophys. J.* 88:505–514.

51. Stricker, J., P. Maddox, …, H. P. Erickson. 2002. Rapid assembly dynamics of the *Escherichia coli* FtsZ-ring demonstrated by fluorescence recovery after photobleaching. *Proc. Natl. Acad. Sci. USA.* 99:3171–3175.

52. Romberg, L., and T. J. Mitchison. 2004. Rate-limiting guanosine 5′-triphosphate hydrolysis during nucleotide turnover by FtsZ, a prokaryotic tubulin homologue involved in bacterial cell division. *Biochemistry.* 43:282–288.

53. Dajkovic, A., G. Lan, …, J. Lutkenhaus. 2008. MinC spatially controls bacterial cytokinesis by antagonizing the scaffolding function of FtsZ. *Curr. Biol.* 18:235–244.

54. Huecas, S., O. Llorca, …, J. M. Andreu. 2008. Energetics and geometry of FtsZ polymers: nucleated self-assembly of single protofilaments. *Biophys. J.* 94:1796–1806.

55. Popp, D., M. Iwasa, …, Y. Maéda. 2009. FtsZ condensates: an in vitro electron microscopy study. *Biopolymers.* 91:340–350.

56. Lan, G., A. Dajkovic, …, S. X. Sun. 2008. Polymerization and bundling kinetics of FtsZ filaments. *Biophys. J.* 95:4045–4056.

57. Surovtsev, I. V., J. J. Morgan, and P. A. Lindahl. 2008. Kinetic modeling of the assembly, dynamic steady state, and contraction of the FtsZ ring in prokaryotic cytokinesis. *PLOS Comput. Biol.* 4:e1000102.

58. Frieden, C., and D. W. Goddette. 1983. Polymerization of actin and actin-like systems: evaluation of the time course of polymerization in relation to the mechanism. *Biochemistry.* 22:5836–5843.

59. Sept, D., J. Xu, …, J. A. McCammon. 1999. Annealing accounts for the length of actin filaments formed by spontaneous polymerization. *Biophys. J.* 77:2911–2919.

60. Falzone, T. T., M. Lenz, …, M. L. Gardel. 2012. Assembly kinetics determine the architecture of α-actinin crosslinked F-actin networks. *Nat. Commun.* 3:861.

61. Mateos-Gil, P., A. Paez, …, M. Vélez. 2012. Depolymerization dynamics of individual filaments of bacterial cytoskeletal protein FtsZ. *Proc. Natl. Acad. Sci. USA.* 109:8133–8138.

62. Lutkenhaus, J. 2007. Assembly dynamics of the bacterial MinCDE system and spatial regulation of the Z ring. *Annu. Rev. Biochem.* 76:539–562.

63. Zhang, Z., J. J. Morgan, and P. A. Lindahl. 2014. Mathematical model for positioning the FtsZ contractile ring in *Escherichia coli*. *J. Math. Biol.* 68:911–930.

64. Romberg, L., M. Simon, and H. P. Erickson. 2001. Polymerization of Ftsz, a bacterial homolog of tubulin. Is assembly cooperative? *J. Biol. Chem.* 276:11743–11753.

65. Redick, S. D., J. Stricker, …, H. P. Erickson. 2005. Mutants of FtsZ targeting the protofilament interface: effects on cell division and GTPase activity. *J. Bacteriol.* 187:2727–2736.

66. Andrianantoandro, E., L. Blanchoin, …, T. D. Pollard. 2001. Kinetic mechanism of end-to-end annealing of actin filaments. *J. Mol. Biol.* 312:721–730.

67. Fass, J., C. Pak, …, A. Mogilner. 2008. Stochastic simulation of actin dynamics reveals the role of annealing and fragmentation. *J. Theor. Biol.* 252:173–183.

68. Kinosian, H. J., L. A. Selden, …, L. C. Gershman. 1993. Actin filament annealing in the presence of ATP and phalloidin. *Biochemistry.* 32:12353–12357.

69. Murphy, D. B., R. O. Gray, …, T. D. Pollard. 1988. Direct demonstration of actin filament annealing in vitro. *J. Cell Biol.* 106:1947–1954.

70. Northrup, S. H., and H. P. Erickson. 1992. Kinetics of protein-protein association explained by Brownian dynamics computer simulation. *Proc. Natl. Acad. Sci. USA*. 89:3338–3342.

71. Choi, T., M. R. Maurya, …, S. Subramaniam. 2010. Stochastic hybrid modeling of intracellular calcium dynamics. *J. Chem. Phys.* 133:165101.

72. Choi, T., M. R. Maurya, …, S. Subramaniam. 2012. Stochastic operator-splitting method for reaction-diffusion systems. *J. Chem. Phys.* 137:184102.

73. Fischer-Friedrich, E., B. M. Friedrich, and N. S. Gov. 2012. FtsZ rings and helices: physical mechanisms for the dynamic alignment of biopolymers in rod-shaped bacteria. *Phys. Biol.* 9:016009.

74. Fischer-Friedrich, E., and N. Gov. 2011. Modeling FtsZ ring formation in the bacterial cell-anisotropic aggregation via mutual interactions of polymer rods. *Phys. Biol.* 8:026007.

75. Masuda, H., Q. Tan, …, M. Inouye. 2012. YeeU enhances the bundling of cytoskeletal polymers of MreB and FtsZ, antagonizing the CbtA (YeeV) toxicity in *Escherichia coli*. *Mol. Microbiol.* 84:979–989.

76. Alberts, B., A. Johnson, …, P. Walter. 2014. Molecular Biology of the Cell, 6th Ed. Garland Science, New York.

77. Needleman, D. 2015. The material basis of life. *Trends Cell Biol.* 25:713–716.

78. Swanson, D., and N. S. Wingreen. 2011. Active biopolymers confer fast reorganization kinetics. *Phys. Rev. Lett.* 107:218103.

79. Wegner, A. 1976. Head to tail polymerization of actin. *J. Mol. Biol.* 108:139–150.

80. Pantaloni, D., C. Le Clainche, and M.-F. Carlier. 2001. Mechanism of actin-based motility. *Science.* 292:1502–1506.

81. Qian, H. 2005. Cycle kinetics, steady state thermodynamics and motors—a paradigm for living matter physics. *J. Phys. Condens. Matter.* 17:S3783–S3794.

82. Qian, H. 2007. Phosphorylation energy hypothesis: open chemical systems and their biological functions. *Annu. Rev. Phys. Chem.* 58:113–142.